International Journal of Non–Linear Mechanics 162 (2024) 104727

Contents lists available at ScienceDirect

International Journal of Non-Linear Mechanics

journal homepage: www.elsevier.com/locate/nlm

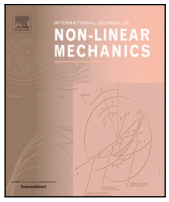

Swelling-driven soft elastic catapults

M. Curatolo [a], G. Napoli [b,*], P. Nardinocchi [c], S. Turzi [d]

[a] Dipartimento di Architettura, Università Roma Tre, Roma, Italy
[b] Dipartimento di Matematica e Applicazioni "Renato Caccioppoli", Università degli Studi di Napoli "Federico II", Napoli, Italy
[c] Dipartimento di Ingegneria Strutturale e Geotecnica, Sapienza Università di Roma, Roma, Italy
[d] Dipartimento di Matematica, Politecnico di Milano, Milano, Italy

ARTICLE INFO

Keywords:
Soft catapult
Differential swelling
Elastica
Stress-diffusion theory

ABSTRACT

The paper outlines and analyzes the conditions for optimizing a catapult mechanism that emerges in a soft rod, initially completely adhered to a rigid lubricated substrate, as a result of oil absorption. Oil diffusion causes differential swelling across the rod thickness, inducing rod bending that is counteracted by adhesion to the substrate. The effect culminates in a gradual detachment of the rod from the substrate, followed by a rapid shooting phase when one end detaches. To elucidate this intricate phenomenon, we employ a modified Euler elastica model that incorporates two additional parameters: the *spontaneous stretching* λ, that quantifies the relative elongation of the material with respect to its dry, unstressed configuration, and the *spontaneous curvature*, c_o, that captures the rod tendency to deflect due to diffusion-induced non-uniform stretching through the thickness. The interrelated parameters, λ and c_o, which evolve over time as they are influenced by the diffusion process are then calculated numerically with a FEM code that combines the finite elasticity model with the Flory–Rehner diffusion model. Finally, we present a comprehensive optimization study of the catapult based on its geometric and material properties, providing insights for the design and control of this novel mechanism.

1. Introduction

Catapults are mechanisms that are used both in biology and in technology to launch a payload by storing elastic energy through deformation. In technology, the primary energy storage mechanisms are tension, torsion, and gravity, which have been used since ancient times. Catapults can be composed of rigid and compliant elements [1]. In biology, elastic energy is stored as a result of deformation, which can be caused by a variety of factors, including changes in air conditions and other atmospheric agents. Biological catapults produce a shooting mechanism that is used for a variety of purposes, including prey capture and defense [2].

Traditionally, man-made catapults were equipped with a crossbar to halt the motion and make the catapult effective. In biology, the energy-storing process is halted by a breaking mechanism that also facilitates the rapid release of stored energy, thus initiating the firing mechanism. In the well-known example of fern sporangia, the catapult serves to disperse spores, and the breaking mechanism is water cavitation within the cells of the spherical capsule enclosing the spores [3,4].

As noted in Ref. [1], the shift from conventional to soft robotics necessitates the design of soft devices for cutting-edge applications. Soft catapults may represent a frontier and demand appropriate nonlinear mechanical models to be characterized. In Ref. [1], gravity is utilized to initiate the deformation process and induce snap instability, thereby creating an elastic catapult. In contrast, our study employs swelling and adhesion as the two key mechanisms to initiate deformation and achieve an elastic catapult through mechanical instability. In particular, the swelling of a rod adhered to a substrate by capillarity, and its subsequent detachment from that substrate, are the physical processes that generate the catapult mechanism. The diffusion of hexane oil, spread across the rigid substrate supporting the rod, permeates the thickness of the rod, creating a differential swelling effect. This differential swelling causes the rod to lose its straight and fully adherent configuration, inducing it to bend and partially detach from the substrate. The bending progresses, resulting in the detachment of an increasing portion of the rod's lower surface. Elastic energy is stored within the rod until the detachment of one end from the substrate triggers the catapult configuration.

Therefore, the utilization of a vinyl-polysiloxane rod in conjunction with solvent diffusion exemplifies a novel approach to harnessing high power output in a controlled manner. This mechanism has the potential for diverse applications demanding rapid and precise movements, such as micro-robotics, actuation systems, and biomedical devices. Rigorous

* Corresponding author.
E-mail address: gaetano.napoli@unina.it (G. Napoli).

https://doi.org/10.1016/j.ijnonlinmec.2024.104727
Received 4 January 2024; Received in revised form 5 April 2024; Accepted 6 April 2024
Available online 8 April 2024
0020-7462/© 2024 The Authors. Published by Elsevier Ltd. This is an open access article under the CC BY license (http://creativecommons.org/licenses/by/4.0/).

research and optimization of this system could lead to significant advancements in power delivery and controlled motion, paving the way for groundbreaking technological developments.

Experiments conducted by one of the authors at the Moss Lab, Boston University, have provided valuable insights into the complexities of the physical processes involved in both the catapult and subsequent relaxation mechanisms. Drawing inspiration from studies on growth-induced blisters in beams adhered to flat substrates, as presented in Refs. [5–7], we have investigated our problem through a modified Euler *elastica* model. This model offers a good qualitative description of the phenomenon, highlighting the critical interplay between bending and adhesion energies — the fundamental mechanism underpinning the catapult effect.

Our modified elastica model hinges on *elastocapillary length*, which arises from the ratio of bending stiffness to adhesion energy [8], and the *spontaneous stretching and curvature* of the rod, which trigger the onset of the catapult mechanism. These *spontaneous* stretching and curvature correspond to the swelling-induced deformations in a three-dimensional rod under no external loads or constraints. While explicit, albeit approximate, formulas exist for bilayer beams, where swelling represents the steady-state configuration [9]; they can be considered generalizations of the well-known Timoshenko formula for bi-metal strip bending [10]. However, to our knowledge, comparable formulas for the time-dependent deformations caused by differential swelling across the thickness of a homogeneous rod or plate are only available for small deformations (see [11] for rods and [12] for plates).

However, incorporating the finite bending induced by swelling within the transient regime remains an open question for future investigations. In this work, we address a catapult mechanism described by: (i) a fully three-dimensional mechanochemical coupling theory that captures the time-dependent stretching and bending caused by swelling in a homogeneous, unconstrained rod, and (ii) the elastica model, which utilizes the intrinsic stretching and bending identified in step (i).

Our analysis begins with a rod initially straight and uniformly expanded compared to its dry state. A key parameter is the chemical potential μ_o of the liquid within the rod, along with the dry thickness h of the rod. Differential swelling is triggered by oil diffusing across the rod's thickness. This oil is assumed to be uniformly distributed on the bottom face, where it contacts the wet substrate. The control parameter is the external chemical potential at the bottom face, which transitions from an initial value μ_o, representing the initial equilibrium state, to a final state μ_e according to a specified time-dependent profile.

A fully three-dimensional, non-linear finite element method (FEM) based model numerically captures the rod's stretching and bending behaviour for various thicknesses and initial conditions. These values are subsequently incorporated into the modified elastica model, where they represent the spontaneous stretching and curvature of the rod. By leveraging the interplay between these two models, we can investigate the conditions that optimize the catapult mechanism, which is the primary focus of this study.

The paper is structured as follows: Section 2 presents a prototypical experiment, selected from those conducted in the Lab. Section 3 provides an initial, rudimentary interpretation of the experiment based on the elastica model. Section 4 briefly outlines the modelling of the mechano-diffusion coupling and the differential swelling of a rod that is free to deform according to the swelling process. In Section 5, the findings derived from combining the two models are presented, and the optimal conditions for creating a soft catapult are discussed.

2. Insight into the catapult from experiments

A catapult mechanism is constructed using a vinyl-polysiloxane rod securely fastened to an acrylic substrate at its right end with a strong adhesive. Dry length L, width b and thickness h of the rod are $0.05 \times 0.01 \times 0.0015$ m. A payload of 0.4 g is encased within a small acrylic hollow cube situated on the beam's left side (see Fig. 1). Liquid hexane is applied to the acrylic substrate's surface using a syringe to facilitate wetting.

The catapult mechanism is initiated by the diffusion of liquid through the rod's thickness. This differential swelling subsequently dictates the rod's bending, overcoming the adhesive forces that maintain its adherence to the substrate. The design hinges on a critical balance between two opposing effects. Adhesive forces act to maintain the rod's attachment to the substrate, while the elastic energy stored within the bent rod counteracts this adhesion, ultimately driving detachment. This interplay between forces leads to a progressive bending distortion that culminates in the rapid and complete release of the rod.

Upon the evaporation of the hexane, the rod returns to its dry, straight form. The entire process, from the initial wetting stage to the complete drying of the rod, takes approximately twenty minutes. This extended duration reflects the gradual diffusion and subsequent evaporation of the hexane solvent. This allows the rod to undergo the desired bending and then return to its original configuration once the solvent has fully dissipated.

Fig. 1 illustrates the complete dynamic behaviour of the vinyl-polysiloxane rod catapult. Two distinct phases are evident. The first phase, lasting from 0 to 230 s, encompasses the slow initial dynamics associated with the absorption of liquid hexane. This absorption leads to buckling of the vinyl-polysiloxane rod, which accumulates elastic energy that is subsequently converted into kinetic energy upon detachment of the left end of the beam. The second phase comprises the slow relaxation process that returns the rod to its initial configuration.

3. An elastica model for the catapult

The key interpretation of the experiment relies on the following concepts. Initially, the rod is straight and in contact with hexane at its bottom face and air at its top face. As hexane diffuses through the rod from the bottom face, it induces a longitudinal stretch and, owing to the differential swelling across the thickness, a curvature. This longitudinal stretch is impeded, causing the beam to experience compression with a non-zero curvature. This compression is eventually released by relinquishing the straight configuration.

Through a modified Euler *elastica*, we can assess the total energy $\mathcal{W}$ associated with the partially buckled configuration of the rod. As the rod releases its compression energy during buckling, we can postulate that the rod is inextensible and unshareable with assigned length L, implying that the stored energy is primarily attributed to bending and adhesion.

We assume that there is no deformation in z direction, so that the longitudinal profile of the rod can be regarded as an unstretchable and flexible strip belonging to the (x, y)-plane. This is represented by a parametric curve $\mathbf{r}(s)$ (see Fig. 2), with $s \in [-L/2, L/2]$, where L denotes the length of the strip and s is the arc-length. Assuming the rod exhibits mirror symmetry about the y-axis, we denote with $\bar{s}$ and $\bar{x}$ the arc-length and the abscissa of the detachment point, respectively.

In the plane of the curve, we introduce a Cartesian frame of reference $(O; \mathbf{e}_x, \mathbf{e}_y)$, where O is the origin and $\mathbf{e}_x$, $\mathbf{e}_y$ are the unit vectors along, respectively, the x and the y axes. We parameterize the tangent and the normal unit vectors by

$$\mathbf{t}(s) = \cos\theta(s)\mathbf{e}_x + \sin\theta(s)\mathbf{e}_y, \qquad \mathbf{n}(s) = -\sin\theta(s)\mathbf{e}_x + \cos\theta(s)\mathbf{e}_y$$

and, hence, $\mathbf{e}_z = \mathbf{t} \times \mathbf{n}$. The end points of the curve are placed at $(-a, 0)$ and $(a, 0)$, so that the stretching, possibly due to swelling,

$$\lambda = \frac{L}{2a}, \tag{3.1}$$

measures the rod excess-length with respect to the dry length.

The energy functional consists of two terms: $\mathcal{W} = \mathcal{W}_f + \mathcal{W}_a$. The first contribution $\mathcal{W}_f$ comes from the energy of the buckled region and it is only due to bending

$$\mathcal{W}_f = \int_0^{\bar{s}} k(\theta' - c_o)^2 \mathrm{d}s, \tag{3.2}$$

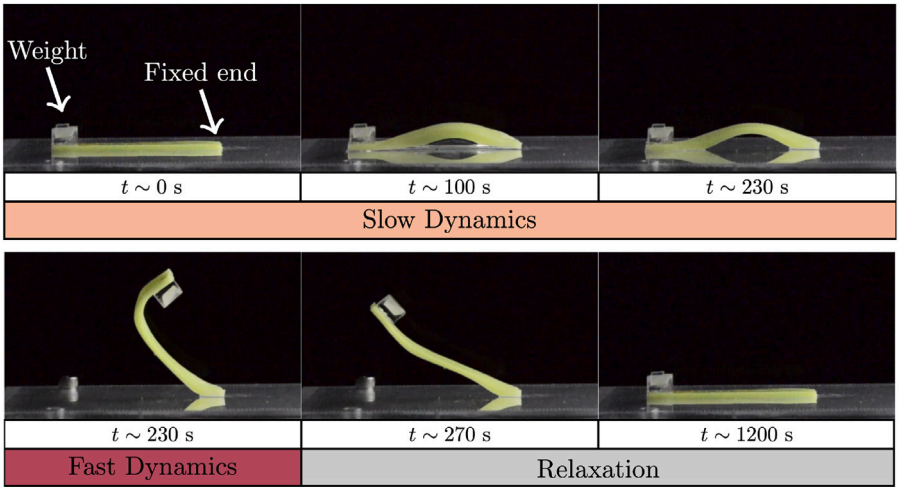

Fig. 1. Dynamics of a vinyl-polisiloxane catapult during absorption of liquid hexane.

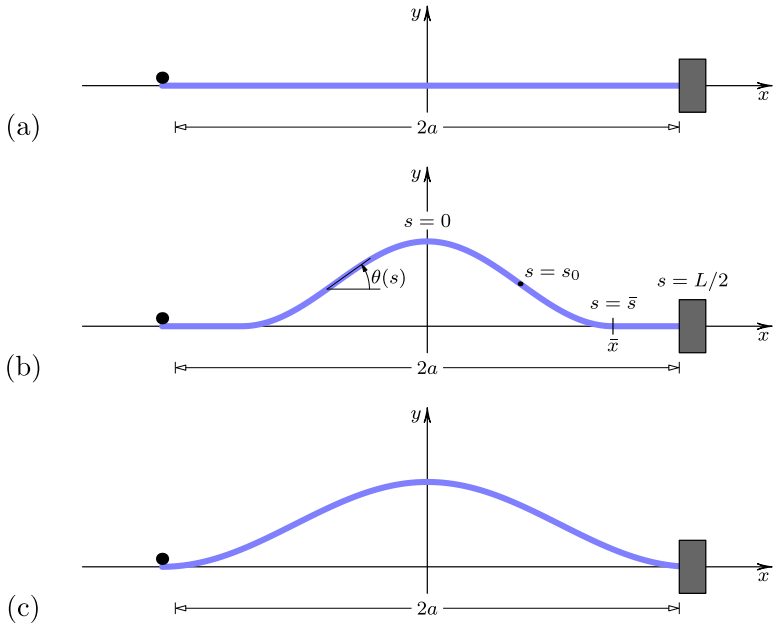

Fig. 2. Schematic representation of swelling-induced deformation of a rod with a clamped right end and a weight on the left end. During deformation, the distance between the two ends of the rod remains constant at $2a$. (a) Dry (reference) configuration: The rod has a length of $L = 2a$. (b) Partially and symmetrically detached configuration: The rod has two separate, adhered parts of finite length. (c) Limit configuration before shooting: Only the two ends of the rod remain in contact with the substrate.

where k is the bending stiffness and c_o is the *constant* spontaneous curvature, possibly induced by swelling. The second term $\mathcal{W}_a$ is related to the adhered region, where we have to consider the contribution of the rod-substrate adhesion energy, of constant density w, which is assumed to be proportional to the length of the adhered curve. Thus, we posit the following energy for the adhered region

$$\mathcal{W}_a = \int_{\bar{s}}^{L/2} (kc_o^2 - 2w)\mathrm{d}s. \tag{3.3}$$

The presence of adhesion introduces a further characteristic length, namely the *elasto-capillary* length, that relates the bending stiffness and the adhesion energy

$$\ell_{ec} := \sqrt{\frac{k}{w}}. \tag{3.4}$$

Standard methods in the calculus of variations allow us to derive the equilibrium equation for the free part of the beam [5,6]

$$k\theta'' - N_x \sin\theta = 0, \qquad s \in [0, \bar{s}) \tag{3.5}$$

where N_x is the unknown horizontal component of the internal force. The boundary conditions are (see Ref. [6]) $\theta(0) = 0$, $\theta(\bar{s}) = 0$, and the transversality condition [13] is

$$k[\theta'(\bar{s})]^2 = 2w. \tag{3.6}$$

Under the assumption of negligible gravity and symmetric solution, it can be shown that the vertical internal force, N_y, is zero throughout the rod. Consequently, it does not contribute to Eq. (3.5). Also the constant spontaneous curvature c_o does not explicitly appear in Eqs. (3.5), (3.6). The variational procedure, detailed in [14], shows that a constant curvature does not appear in both the Euler–Lagrange equation and the boundary conditions. However, c_o contributes in an essential way to the evaluation of the energy.

A last additional condition is derived from the geometric identity that links $\bar{x}$ to $\bar{s}$: $a = \bar{x} + L/2 - \bar{s}$, that is

$$\bar{s} = \bar{x} + (\lambda - 1)a. \tag{3.7}$$

This identity can be equivalently written in terms of the function $\theta(s)$,

$$\bar{s} = \int_0^{\bar{s}} \cos\theta \, \mathrm{d}s + (\lambda - 1)a. \tag{3.8}$$

Overall, our problem has one unknown function, $\theta(s)$, and two unknown constants, N_x and $\bar{s}$.

3.1. Analytic solution and stored elastic energy

It is well known that the elastica Eq. (3.5) can be solved in terms of elliptic functions. To this end, let us rewrite Eq. (3.5) as follows

$$\theta'' + \tau \sin\theta = 0, \tag{3.9}$$

where $\tau := -N_x/k$. A first integral is

$$(\theta')^2 = 2\tau(\cos\theta - \cos\theta_0), \tag{3.10}$$

where $\theta_0 := \theta(s_0)$ is the minimum value of θ in the range $[0, \bar{s}]$, that is $s = s_0$ is the right inflection point of the rod (see Fig. 2). Thus, we can use the transversality condition (3.6) together with (3.10) to eliminate τ in favour of θ_0

$$\tau = \ell_{ec}^{-2} \left(1 - \cos\theta_0\right)^{-1}. \tag{3.11}$$

Eq. (3.10) reduces to

$$\theta' = \pm \ell_{ec}^{-1} \sqrt{\frac{2(\cos\theta - \cos\theta_0)}{1 - \cos\theta_0}}, \tag{3.12}$$

where the sign $-$ (respectively, $+$) is to be used in the interval $s \in (0, s_0)$ (respectively, $s \in (s_0, \bar{s})$). Eq. (3.12) is an ordinary differential equation that can be solved by separation of variables. The solution is

$$\bar{s} = -2\sqrt{2}\,\ell_{ec} \mathrm{F}\big(\theta_0/2; \csc^2(\theta_0/2)\big), \tag{3.13}$$

where F denotes the incomplete elliptic integral of first kind [15].

Similarly, we can exploit Eq. (3.12) to compute $\bar{x}$, the abscissa of the detachment point $\bar{x} := \int_0^{\bar{s}} \cos\theta \, \mathrm{d}s$. With the help of Eqs. (3.12) and (3.13), we obtain

$$\bar{x} = \bar{s}\cos\theta_0 - 2\sqrt{2}\ell_{ec}(1 - \cos\theta_0)\mathrm{E}\big(\theta_0/2; \csc^2(\theta_0/2)\big), \tag{3.14}$$

where E represents the incomplete elliptic integral of second kind [15].

Finally, Eq. (3.7) yields a third identity that involves both $\bar{s}$ and $\bar{x}$. Hence, we have a systems of three nonlinear transcendental equations, namely Eqs. (3.13), (3.7) and (3.14), whose solutions provide the values at equilibrium of $\bar{s}$, $\bar{x}$ and θ_0, as functions of ℓ_{ec} and λ.

Also the total stored energy can be written in terms of $\bar{s}$, $\bar{x}$ and θ_0. Indeed, it can be shown that, through skilful use of the first integral (3.12), we arrive at

$$\mathcal{W} = \frac{2k}{\ell_{ec}^2}\left(\frac{\bar{x} - \bar{s}\cos\theta_0}{1 - \cos\theta_0} + \bar{s} - \lambda a\right) + k c_o^2 \lambda a. \tag{3.15}$$

3.2. Shooting condition

The limiting configuration immediately prior to launch, depicted in Fig. 2(c), occurs when the rod maintains contact with the platform only at its two endpoints, so that $\bar{x} = a$. Upon release, the left end detaches, launching the weight, while the right end remains clamped.

The effectiveness of the catapult depends on the interplay between its length, elasticity, and surface tension. This interplay is quantified by the ratio between the elastocapillary length, ℓ_{ec}, and a. When $\ell_{ec} \gg a$, the adhesion forces are weak so that the beam undergoes an Euler-type instability as soon $L > 2a$ and the beam globally detaches from the surface with only the end-points attached. In such a case, not enough elastic energy is stored and the catapult cannot develop. By contrast, when $\ell_{ec} \ll a$, the adhesion is so strong that the beam may never fully detach from the surface and the limiting situation $\bar{x} = a$ may never be reached.

The previous analysis shows that the optimal catapult must occur in an intermediate regime of adhesion, in which the contact point $\bar{x}$ gradually moves towards $x = a$ as λ increases. We assume quasi-static conditions, so that the dynamics of the beam is described by a sequence of equilibrium states. In this regime, the transition to a completely detached circular configuration with radius $1/c_o$, and thus the development of a shooting phase, can be assumed to occur when the buckled solution is no longer favoured by adherence with the substrate, i.e. when $\bar{x} = a$.

In this case, the three Eqs. (3.13),(3.14), and (3.7), with $\bar{x} = a$, can be used to derive $\bar{s}$, θ_0 and λ at the moment of shooting. After some algebra, these read

$$\lambda + 2\sqrt{2}\,\frac{\ell_{ec}}{a}\mathrm{F}\big(\theta_0/2; \csc^2(\theta_0/2)\big) = 0, \tag{3.16a}$$

$$1 + 2\sqrt{2}\frac{\ell_{ec}}{a}(1 - \cos\theta_0)\mathrm{E}\big(\theta_0/2; \csc^2(\theta_0/2)\big) - \lambda\cos\theta_0 = 0, \tag{3.16b}$$

$$\bar{s}/a - \lambda = 0, \tag{3.16c}$$

where we see that $\bar{s}/a$, θ_0 and λ only depend on the ratio $\eta := \ell_{ec}/a$. The energy stored at the moment of shooting, calculated as given in Eq. (3.15),

$$\frac{\mathcal{W}_s}{k/a} = \frac{2\,a^2}{\ell_{ec}^2}\left(\frac{1 - \lambda\cos\theta_0}{1 - \cos\theta_0}\right) + \lambda(c_o a)^2, \tag{3.17}$$

depends only on two dimensionless groups, $\eta := \ell_{ec}/a$ and $\gamma := c_o a$. We notice that, by Eqs. (3.16), $\bar{s}/a$, θ_0 and λ do not depend on γ, but are only functions of η.

In agreement with our initial intuition, it is not possible to find a solution to the Eqs. (3.16) if the adhesion is too strong. Indeed, if we derive λ from (3.16a) and substitute it into (3.16b), we can easily obtain η as a function of θ_0. Similarly, by obtaining η from (3.16a), we get $\lambda = \lambda(\theta_0)$ from (3.16b). The functions $\eta = \eta(\theta_0)$ and $\lambda = \lambda(\theta_0)$ are explicitly given by

$$\eta = \frac{1}{2\sqrt{2}}\Big[(\cos(\theta_0/2) - 1)\mathrm{E}\big(\theta_0/2; \csc^2(\theta_0/2)\big) - \cos(\theta_0/2)\mathrm{F}\big(\theta_0/2; \csc^2(\theta_0/2)\big)\Big]^{-1}, \tag{3.18}$$

$$\lambda = \left(\cos(\theta_0/2) - \frac{(\cos(\theta_0/2) - 1)\mathrm{E}\big(\theta_0/2; \csc^2(\theta_0/2)\big)}{\mathrm{F}\big(\theta_0/2; \csc^2(\theta_0/2)\big)}\right)^{-1}, \tag{3.19}$$

and are plotted in Fig. 3.

We note that there are generally two distinct equilibrium solutions, corresponding to two distinct values of θ_0, for $\eta > \eta_{\min}$, and there are no solutions when $\eta < \eta_{\min}$, with $\eta_{\min} \approx 0.5427$. This sets a lower bound for the elasto-capillary length (and an upper bound for the adhesion strength) so that it must be $\ell_{ec} \gtrsim 0.5427\,a$. Among the two possible solutions for θ_0, we select the one with the smaller absolute value of the inflection angle, $|\theta_0|$. As shown in Fig. 3, this solution corresponds to smaller values of the stretching parameter λ. Intuitively, we imagine that during a growth process driven by absorption from the dry state, the solution with less stretching is the one that physically manifests first.

When η and γ are taken to be independent parameters, $\mathcal{W}_s(\eta, \gamma)$ depends quadratically on γ so that the maximum $\mathcal{W}_s(\eta, \gamma)/(k/a)$ is achieved when η is minimum, namely $\eta \approx 0.5427$, and γ is the largest possible (see Fig. 4). However, in a more realistic model, when we consider the absorption of a solvent from the bottom surface, and the corresponding diffusion across the thickness, it is no longer possible to choose η (and thus λ) and γ independently, and γ cannot be arbitrarily large.

This observation highlights the need to identify an alternative source for this information, as it establishes the coupling between λ and γ. Consequently, we can then evaluate the energy stored at the moment of launch by a swelling-driven catapult mechanism. Before proceeding with the following sections, let us discuss the most suitable method for non-dimensionalizing the stored energy, $\mathcal{W}_s$.

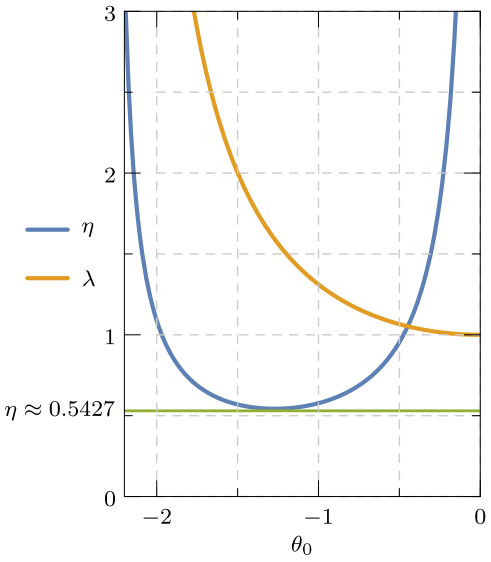

Fig. 3. Plot of the functions $\eta = \eta(\theta_0)$ and $\lambda = \lambda(\theta_0)$ as given in Eqs. (3.18), (3.19). The green line shows the limit value $\eta \approx 0.5427$.

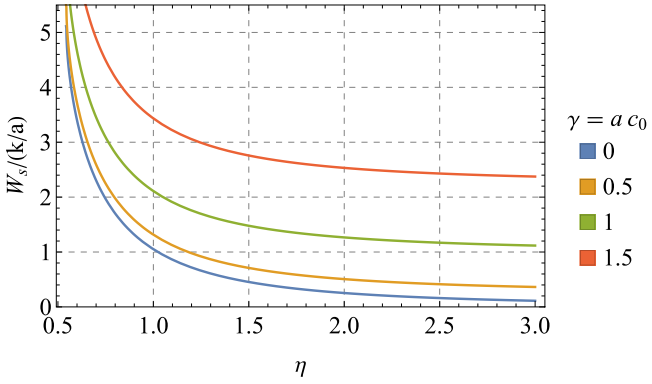

Fig. 4. Profile of the stored energy at the moment of shooting (defined by $\bar{x} = a$), as a function of $\eta = \ell_{ec}/a$, for different values of $\gamma = 0; 0.5; 1; 1.5$, as given in Eq. (3.17). The limit value $\eta \approx 0.5427$ is clearly shown by the steep profile of the energy.

Remark. The ratio of the stored elastic energy $\mathcal{W}_s$ with k/a, as provided in Eq. (3.17), is valuable for comparing different scenarios where the rod bending modulus k remains constant but, for instance, the adhesion strength w varies. By contrast, if we aim to compare situations where w is fixed but, for example, the thickness of the rod, and consequently, the bending modulus, is modified, a more suitable metric is the ratio of $\mathcal{W}_s$ to the *interface energy*, $2aw$. This is because the interface energy depends only on the adhesion strength and on the length of the interface, whereas is independent of the bending modulus. In this last scenario, Eq. (3.17) rewrites as

$$\frac{\mathcal{W}_s}{2aw} = \frac{1 - \lambda \cos\theta_0}{1 - \cos\theta_0} + \frac{1}{2}\lambda\gamma^2\eta^2. \tag{3.20}$$

4. Determining the spontaneous curvature and stretching of the rod

We assume that c_o and λ in the modified elastica model are determined by the swelling-induced curvature and stretching obtained in the FEM simulations of a three-dimensional rod under no external forces or constraints. This relationship forms the foundation of the two-level elastic catapult model. First, a three-dimensional rod stress-diffusion model is simulated numerically to obtain thickness-dependent values for swelling-induced bending and stretching. These values then serve as inputs to a one-dimensional elastica model, which determines the rod's shape and characterizes its energy state relevant to the catapult mechanism.

4.1. The equations of the stress-diffusion model

The stress-diffusion model employed for our analysis has been previously introduced in various publications by some of the Authors [9,16,17]. Here, we provide a concise overview of the model's application to a soft rod on a wet substrate. As established in the literature, diffusion of a fluid across the rod's thickness induces differential swelling, leading to rod bending [18,19]. However, unlike typical scenarios reported in the literature, our rod is fabricated from a homogeneous material, resulting in transient bending. Ultimately, the rod reverts to its straight configuration, albeit with a permanent increase in length.

To better understand the influence of curvature and stretching, we disregard the laboratory setup's clamp and the adhesive interaction between the rod and the wet substrate. We consider the rod to be free to adopt its deformed configuration, with longitudinal axis stretching and curvature denoted by λ and c_o, respectively. No additional constraints are imposed, and the values of (λ, c_o) at any point during the swelling process are determined by solving the corresponding stress-diffusion problem.

The dynamics of the swelling process is governed by the balance equations for forces and solvent, the thermodynamic inequalities that restrict the class of admissible constitutive prescriptions, and a free energy that encompasses both elastic and mixing contributions. All these elements define a set of equations (see [9,16,17] for details) in the state variables c_d and $\mathbf{u}$, which are the solvent concentration field per unit dry volume and the displacement from the reference dry configuration $\mathcal{B}$, which is also the domain of computation:

$$\mathrm{div}\,\mathbf{S} = \mathbf{0} \quad \text{and} \quad \dot{c}_d = -\mathrm{div}\,\mathbf{h}, \quad \text{on} \quad \mathcal{B}\times\mathcal{I}, \tag{4.21}$$

$$\mathbf{S}\,\mathbf{m} = \mathbf{s} \quad \text{and} \quad -\mathbf{h}\cdot\mathbf{m} = q, \quad \text{on} \quad \partial\mathcal{B}\times\mathcal{I}, \tag{4.22}$$

$$\mathbf{S} = G\,\mathbf{F}_d - p\,\mathbf{F}_d^{\star} \quad \text{with} \quad \mathbf{F}_d = \mathbf{I} + \nabla\mathbf{u} \quad \text{and} \quad J_d = \det\mathbf{F}_d, \tag{4.23}$$

$$\mu = \mathcal{R}\,T\left(\log\frac{J_d - 1}{J_d} + \frac{1}{J_d} + \frac{\chi}{J_d^2}\right) + p\,\Omega, \tag{4.24}$$

$$\mathbf{h} = -\mathbf{M}(\mathbf{F}_d, c_d)\nabla\mu \quad \text{with} \quad \mathbf{M}(\mathbf{F}_d, c_d) = \frac{D}{\mathcal{R}T}\,c_d\mathbf{C}_d^{-1}. \tag{4.25}$$

Therein, $\mathbf{S}$ represents the reference stress and $\mathbf{h}$ the solvent flux per unit reference volume; $\mathbf{s}$ denotes the boundary traction and q the rate of solvent transported into $\mathcal{B}$ across its boundary $\partial\mathcal{B}$; $\mathbf{C}_d = \mathbf{F}_d^T\mathbf{F}_d$ represents the strain tensor, Ω the molar volume of the water, $\mathcal{R}$ the gas constant, T the ambient temperature, G the shear modulus and D the liquid diffusivity within the gel. Finally, p the is the reactive stress field which enforces the incompressibility constraint between the state variables:

$$J_d = \det\mathbf{F}_d = \hat{J}_d(c_d) = 1 + \Omega c_d. \tag{4.26}$$

4.2. The free and bent rod

To solve the problem, we assume that the entire rod boundary is impermeable except for the bottom face. Here, a chemical equilibrium condition is assumed to prevail at all times. Specifically, the chemical potential μ of the solvent in the gel rod is equal to the chemical potential of the pure solvent, which is zero. We further assume that the chemical boundary condition on the bottom face persists throughout the process. This applies before the onset of diffusion due to contact with the wet substrate, and even after the rod detaches from the substrate, as the bottom face remains wet (see Fig. 5, panel d). Therefore, we write:

$$q = 0 \quad \text{on} \quad \partial\mathcal{B}/\mathcal{F}_b \quad \text{and} \quad \mu = 0 \quad \text{on} \quad \mathcal{F}_b, \tag{4.27}$$

where $\mathcal{F}_b$ identifies the bottom face of the rod.

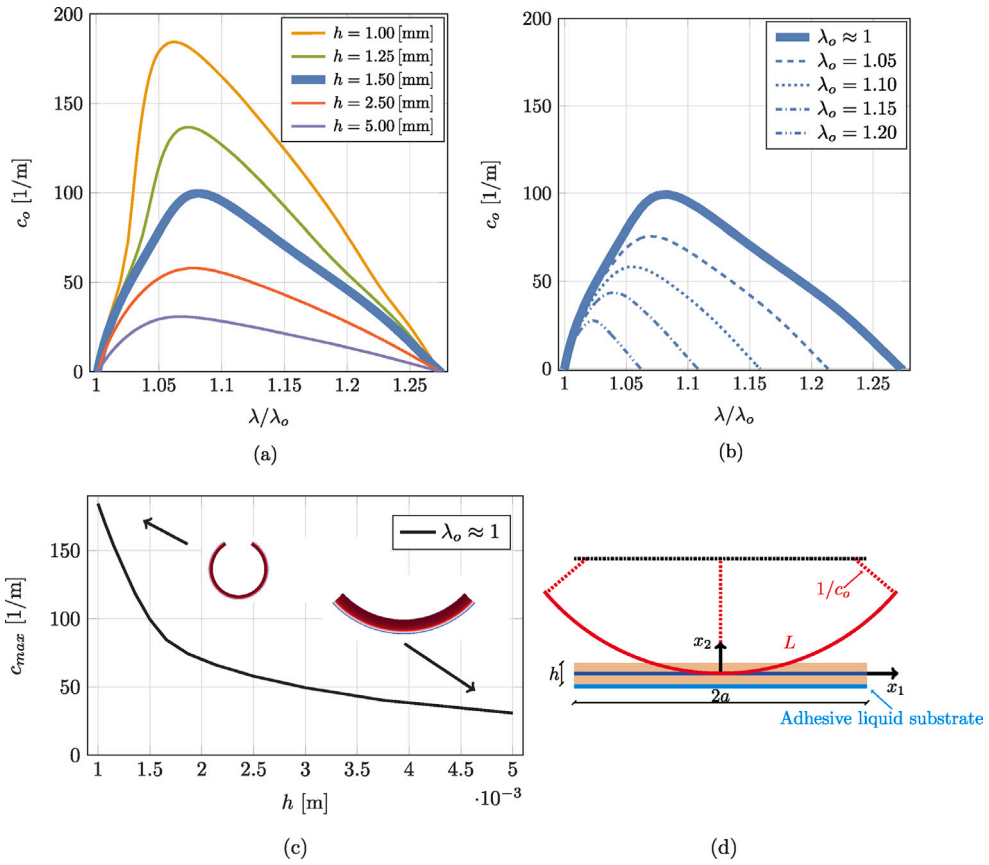

Fig. 5. (a) Curvature c_o and stretch λ/λ_o for a sample with $\lambda_o \approx 1$ and $\mu_o = -10500$ J/mol and different rod thicknesses. (b) Curvature c_o and stretch λ/λ_o for a sample with $h = 1.5$ mm and different initial stretch and chemical potential pairs λ_o, μ_o. (c) Maximum curvature c_{max} for $\mu_o = -10500$ J/mol and different values of h. Insets show the deformed configuration corresponding to different thicknesses. (d) Initial straight (light brown) and intermediate bent configuration of the free rod during absorption of liquid hexane (cyan layer); the solid blue and red line represent the rod axis before diffusion starts and in the bent configuration.

We assume that the initial configuration of the rod corresponds to a straight, homogeneous, and freely slightly swollen state. Therefore, the initial free-swelling stretch, denoted by λ_o, is governed by the equation:

$$\log\left(1-\frac{1}{\lambda_o^3}\right)+\frac{1}{\lambda_o^3}+\frac{\chi}{\lambda_o^6}+\frac{m}{\lambda_o}=\frac{\mu_o}{\mathcal{R}T}\,, \tag{4.28}$$

with $m := G\Omega/RT$. Then, the length L of the bent rod axis is given by $L = (\lambda/\lambda_o)\,2a$.

To give an example, if we fix $G = 2\cdot 10^6$ Pa and $\chi = 0.4$, for $\mu_o = -10500, -1800, -815, -415, -220$ J/mol, we obtain $\lambda_o = 1.001, 1.05, 1.10, 1.15, 1.20$.

Furthermore, by fixing the diffusivity, D, and the initial conditions, we can investigate the swelling dynamics. In particular, let u and w represent the longitudinal and transverse components of the displacement vector $\mathbf{u}$, respectively. Then, for any given time t, the curvature c_o and the stretching λ achieved by the rod can be evaluated using the following expressions:

$$c_o = \frac{w''(1+u') - w'u''}{((1+u')^2 + w'^2)^{3/2}} \quad \text{and} \quad \lambda = (C_{11}(x_1,0,0))^{1/2}\,, \tag{4.29}$$

respectively, being $u(x_1) = \mathbf{u}(x_1,0,0)\cdot\mathbf{e}_1$, $w(x_1) = \mathbf{u}(x_1,0,0)\cdot\mathbf{e}_2$.

We now fix the material parameters $G = 2\cdot 10^6$ Pa, $\chi = 0.4$ and $D = 10^{-8}$ m^2/s. Fig. 5 presents the solution of the 3D model in terms of the rod's curvature. The top left panel shows the relationship between natural curvature c_o and stretching λ/λ_o for various rod thicknesses ranging from $h = 1.0$ mm to $h = 5.0$ mm, considering an initial state approaching dryness, namely $\mu_o = -10500$ J/mol and $\lambda_o \approx 1$. The top right panel displays the same relationship under various initial conditions, specifically for different λ_o or, equivalently, μ_o at a fixed thickness $h = 1.5$ mm. As expected, the curvature increases with decreasing thickness (left, progressing from the violet to the orange curve), that is, thinner rods exhibit higher curvatures; it also increases as the initial state becomes drier (right, progressing from the bottom dashed curve to the solid one). Finally, the bottom-left panel of Fig. 5 shows the relationship between the maximum curvature c_{max} attained by the rod and the rod thickness h, under fixed initial conditions $\mu_o = -10500$ J/mol.

It is worth noting that the same study could be extended to investigate different material parameters. However, the current lack of an explicit formula for the swelling-driven transient bending forces hinders the efficient solution within a finite element code, making a parametric analysis computationally expensive.

5. Towards an effective catapult: results and discussion

We define an optimal catapult mechanism as one that maximizes the elastic energy stored within the rod just before detachment. This energy should be effectively released during the launch phase to optimize payload projection. To achieve this, we will investigate how stored elastic energy varies with respect to rod thickness, h, and adhesion energy per unit length, w. We use the expression for elastic energy provided by the elastica model (Eq. (3.17)). Therein, c_o corresponds to the spontaneous curvature calculated within the three-dimensional mechano-chemical problem.

Let us illustrate the results using a specific example based on the rod described in Section 2. Thus, we consider a material with a shear modulus $G = 2\cdot 10^6$ Pa, dry length $2a = 0.05$ m, and rod width $b = 0.01$ m. The swelling-induced length of the rod is denoted by $L = (\lambda/\lambda_o)\,2a$; we assume $\lambda_o = 1$ corresponding to the dry case.

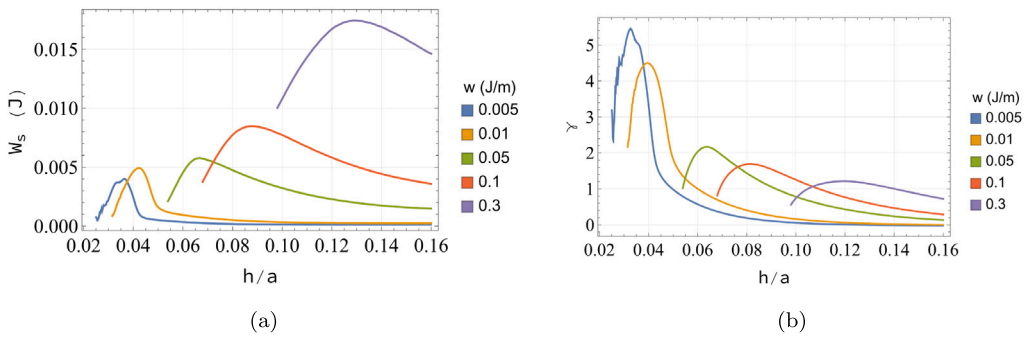

Fig. 6. Stored energy and dimensionless spontaneous curvature as a function of the rod thickness, for different values of the adhesion energy per unit length, w, respectively (a) and (b). The material constants are chosen to reproduce the experimental values, namely, $G = 2 \cdot 10^6$ Pa, $b = 0.01$ m, $2a = 0.05$ m.

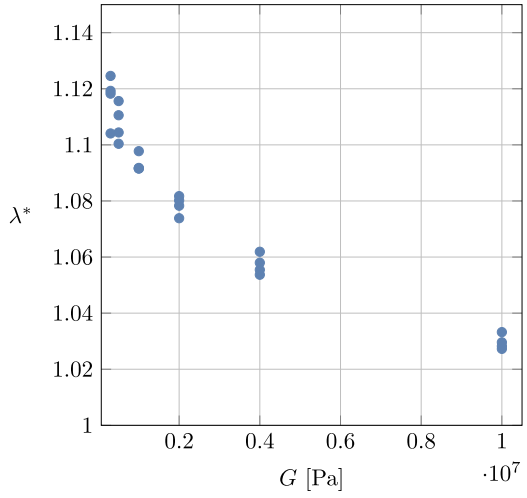

Fig. 7. Stretching value λ^* corresponding at maximum spontaneous curvature c_{max} versus G for different values of the thickness h going from 1.5 mm to 3 mm.

About the parameter h of our study, we have the experimental value $h = 0.0015$ m. This value leads to a bending stiffness $k = EI = \frac{3G}{12} b h^3 \approx 16.9 \cdot 10^{-6}$ Jm, where E is the Young's modulus (assumed related to the shear modulus G). The precise determination of the parameter w can be quite challenging. It hinges on a multitude of factors, including the nature of the contacting materials, surface treatments, temperature, and other variables that often lie beyond our direct control. Based on literature values, we consider a reasonable estimate of $w \approx 0.1$ J/m^2, which corresponds to a characteristic length $\ell_{ec} \approx 0.01$ m as suggested in Refs. [5,20].

As illustrated in Fig. 6, for a given adhesion value w, a specific rod thickness exists that maximizes the stored elastic energy at the point of launch. This observation highlights the importance of careful consideration of the rod's geometrical characteristics beyond the material properties, when designing an effective catapult. Even small deviations in rod thickness can significantly impact the catapult's efficiency in certain cases. By comparing the stored energy in Fig. 6(a) with the calculated spontaneous curvature in Fig. 6(b), we observe that the optimal rod thickness is primarily dictated by the maximum curvature induced by diffusion. This is evident as the peaks of both curves roughly coincide. Therefore, it is critical to determine the solvent diffusion-induced curvature. This can be achieved, either experimentally or numerically, using a sample rod free from external loads or constraints, as detailed in Section 4.

Interestingly, Fig. 5(a) indicates that the maximum energy and maximum spontaneous curvature are achieved at approximately constant stretching values around $\lambda \approx 1.1$, with minimal dependence on the rod thickness h. In general, the stretching value λ^* at which the maximum spontaneous curvature occurs (it is important to note that this maximum curvature is confined to a limited stretching range, as verified numerically) depends on the material's stiffness G: softer materials exhibit a larger λ^*, whereas for stiff materials (high G), λ^* approaches 1. Fig. 7 illustrates the variation of λ^* across a wide range of G values.

Finally, we note that since the stretching, λ, depends solely on the parameter η, as determined by Eq. (3.16), we can leverage the asymptotic analysis of [6] to obtain an approximate formula for λ as a function of η (and vice versa).

$$\lambda \sim 1 + \frac{1}{2\pi^2\eta^2} + \frac{21}{32\pi^4\eta^4}, \tag{5.30}$$

$$\eta \sim \frac{1}{\sqrt{2}\pi\sqrt{\lambda - 1}} + \frac{21\sqrt{\lambda - 1}}{16\sqrt{2}\pi}. \tag{5.31}$$

Therefore, the following formula defines a simple criterion for an effective catapult

$$\sqrt{\frac{G\, b\, h^3}{4w}} \approx \eta^*\, a, \tag{5.32}$$

where η^* is obtained from (5.31) after the substitution of λ with λ^*. In our specific experiment, where $G = 2 \cdot 10^6$ Pa, Eq. (5.31) yields $\eta^* \approx 0.8$ when $\lambda^* = 1.1$.

Eqs. (5.30)–(5.32) drive the design of the catapult mechanism, within the limits of the present model. In particular, Eq. (5.32) delivers a combination of different parameters which can be directly used to define the optimal catapult. The shear modulus G and, in a weaker way, the thickness h affect the stretching value $\lambda^\star$ at which the maximum spontaneous curvature occurs (from Fig. 6). On the other hand, Eq. (5.31) delivers the value of $\eta^\star$ to be used in (5.32), together with a fixed b, to get the optimal adhesion w, that is, the adhesion which makes the catapult effective.

In conclusion, deeper insights could be obtained through an explicit asymptotic analysis of diffusion-induced bending, which would take the place of the numerical analysis and would enable a more comprehensive the parameters-dependent study. However, the explicit analysis of the diffusion-induced bending in rods and plates is still lacking, apart from a few attempts recently developed within the context of a linear mechanical theory [12].

In our opinion, this study establishes a foundational understanding of a new catapult mechanism, which can drive the development of future explicit analyses. We leave this issue for future studies.

CRediT authorship contribution statement

M. Curatolo: Writing – original draft, Software, Investigation, Conceptualization. **G. Napoli:** Writing – original draft, Supervision, Methodology, Investigation, Conceptualization. **P. Nardinocchi:** Writing – original draft, Supervision, Methodology, Investigation, Conceptualization. **S. Turzi:** Writing – original draft, Supervision, Methodology, Investigation, Conceptualization.

Declaration of competing interest

The authors declare that they have no known competing financial interests or personal relationships that could have appeared to influence the work reported in this paper.

Data availability

No data was used for the research described in the article.

Acknowledgements

M.C. acknowledges the Head of the Moss Lab, prof. Douglas Holmes, who hosted him at Boston University and made possible creating the experiments. The work of G.N. and S.T. has been funded by the MUR Project PRIN 2020, Italy, *Mathematics for Industry 4.0*, Project No. 2020F3NCPX. S.T. also acknowledges the partial support by MUR, Italy, grant *Dipartimento di Eccellenza 2023–2027*. P.N. thanks the MUR Project PRIN 2022, *Mathematical Modelling of Heterogeneous Systems*. This manuscript was also conducted under the auspices of the GNFM-INdAM.

References

[1] C. Armanini, F. Dal Corso, D. Misseroni, D. Bigoni, From the elastica compass to the elastica catapult: an essay on the mechanics of soft robot arm, Proc. R. Soc. A: Math., Phys. Eng. Sci. 473 (2198) (2017) 20160870, http://dx.doi.org/10.1098/rspa.2016.0870.

[2] A. Sakes, M. van der Wiel, P.W.J. Henselmans, J.L. van Leeuwen, D. Dodou, P. Breedveld, Shooting mechanisms in nature: A systematic review, PLoS One (7) 1–46, http://dx.doi.org/10.1371/journal.pone.0158277.

[3] X. Noblin, N.O. Rojas, J. Westbrook, C. Llorens, M. Argentina, J. Dumais, The fern sporangium: A unique catapult, Science 335 (6074) (2012) 1322, http://dx.doi.org/10.1126/science.1215985.

[4] C. Llorens, M. Argentina, N. Rojas, J. Westbrook, J. Dumais, X. Noblin, The fern cavitation catapult: mechanism and design principles, J. R. Soc. Interface 13 (114) (2016) http://dx.doi.org/10.1098/rsif.2015.0930.

[5] T.J.W. Wagner, D. Vella, The sticky elastica: delamination blisters beyond small deformations, Soft Matter 9 (2013) 1025–1030, http://dx.doi.org/10.1039/C2SM26916C.

[6] G. Napoli, S. Turzi, The delamination of a growing elastic sheet with adhesion, Meccanica 52 (14) (2017) 3481–3487, http://dx.doi.org/10.1007/s11012-017-0618-0.

[7] G. Napoli, G. Puglisi, Transition between partially and fully delaminated configurations of glued thin films, Appl. Eng. Sci. 9 (2022) 100081, http://dx.doi.org/10.1016/j.apples.2021.100081.

[8] J. Bico, B. Roman, L. Moulin, A. Boudaoud, Elastocapillary coalescence in wet hair, Nature 432 (7018) (2004) 690, http://dx.doi.org/10.1038/432690a.

[9] A. Lucantonio, P. Nardinocchi, M. Pezzulla, Swelling-induced and controlled curving in layered gel beams, Proc. R. Soc. A: Math., Phys. Eng. Sci. 470 (2171) (2014) http://dx.doi.org/10.1098/rspa.2014.0467.

[10] S. Timoshenko, Analysis of bimetal thermostats, JOSA 11 (1925) 233–255.

[11] A. Lucantonio, P. Nardinocchi, Reduced models of swelling-induced bending of gel bars, Int. J. Solids Struct. 49 (11) (2012) 1399–1405, http://dx.doi.org/10.1016/j.ijsolstr.2012.02.025.

[12] Z. Ding, P. Lyu, A. Shi, X. Man, M. Doi, Diffusio-mechanical theory of gel bending induced by liquid penetration, Macromolecules 55 (16) (2022) 7092–7099, http://dx.doi.org/10.1021/acs.macromol.2c01331.

[13] I.M. Gelfand, S.V. Fomin, Calculus of Variations, Prentice Hall, 1963.

[14] R. De Pascalis, G. Napoli, S. Turzi, Growth-induced blisters in a circular tube, Physica D 283 (2014) 1–9, http://dx.doi.org/10.1016/j.physd.2014.05.008.

[15] M. Abramovitz, I.A. Stegun, Handbook of Mathematical Functions. with Formulas, Graphs and Mathematical Tables, Dover, 1964.

[16] A. Lucantonio, P. Nardinocchi, L. Teresi, Transient analysis of swelling-induced large deformations in polymer gels, J. Mech. Phys. Solids 61 (1) (2013) 205–218, http://dx.doi.org/10.1016/j.jmps.2012.07.010.

[17] M. Curatolo, P. Nardinocchi, E. Puntel, L. Teresi, Transient instabilities in the swelling dynamics of a hydrogel sphere, J. Appl. Phys. 122 (14) (2017) 145109, http://dx.doi.org/10.1063/1.5007229.

[18] A. Pandey, D.P. Holmes, Swelling-induced deformations: a materials-defined transition from macroscale to microscale deformations, Soft Matter 9 (2013) 5524–5528, http://dx.doi.org/10.1039/C3SM00135K.

[19] M. Curatolo, P. Nardinocchi, Swelling-induced bending and pumping in homogeneous thin sheets, J. Appl. Phys. 124 (8) (2018) 085108, http://dx.doi.org/10.1063/1.5043580.

[20] D. Vella, J. Bico, A. Boudaoud, B. Roman, P.M. Reis, The macroscopic delamination of thin films from elastic substrates, Proc. Natl. Acad. Sci. 106 (27) (2009) 10901–10906, http://dx.doi.org/10.1073/pnas.0902160106.